Strong-Base Activated Carbons Derived from Recycled CDs and DVDs for Sustainable Wastewater Treatment

Juan Carlos Moreno-Piraján[1]*, Liliana Giraldo[2]

[1]Departamento de Química, Facultad de Ciencias, Grupo de Sólidos Porosos y Calorimetría, Universidad de los Andes, Bogotá, Colombia

[2]Departamento de Química, Grupo de Calorimetría, Facultad de Ciencias, Universidad Nacional de Colombia, Bogotá, Colombia

*Corresponding author: jumoreno@uniandes.edu.co

Abstract

Electronic waste is among the fastest-growing solid waste streams worldwide. Compact discs (CDs) and digital versatile discs (DVDs) alone account for millions of tonnes of discarded polycarbonate-based materials each year, yet effective valorization pathways for these residues remain scarce. In this study, these residues were converted into activated carbons via chemical activation with strong bases (KOH, LiOH, and $Ba(OH)_2$), and the effects of the activating agent on pore structure, surface chemistry, and adsorption performance were systematically investigated. KOH activation produced the most accessible microporous structure, with a BET surface area of approximately 500 m^2/g and a pore system dominated by ultramicropores; $Ba(OH)_2$ yielded materials with more basic surfaces and moderate pore development; and LiOH resulted in the least developed porosity. Despite comparable structural disorder across all samples, adsorption performance was governed primarily by pore accessibility rather than by the degree of graphitic ordering. BTX vapor adsorption capacities followed the order KOH > $Ba(OH)_2$ > LiOH, with KOH-derived carbons benefiting from the combined effect of high micropore accessibility and π–π interactions with aromatic adsorbates. Breakthrough analysis and kinetic modeling confirmed that adsorption dynamics are controlled by the interplay between confinement effects and intraparticle diffusion. These findings establish that polymeric electronic waste can be converted into competitive adsorbents for volatile organic compound removal, providing a quantitative basis for the rational design of waste-derived carbon materials within a circular economy framework.

Keywords: activated carbon; waste valorization; CD/DVD waste; chemical activation; BTX adsorption; volatile organic compounds; e-waste

1. Introduction

Global generation of electrical and electronic equipment waste (WEEE) has reached alarming levels, exceeding 62 million tonnes per year and growing by an estimated 2–3 Mt annually [1, 2]. Among the polymer-based fraction of this stream, optical storage media—compact discs (CDs) and digital versatile discs (DVDs)—occupy a particularly problematic niche: they are composed primarily of polycarbonate with a high carbon content (~85 wt%), coated with metallic and lacquer layers, and largely excluded from conventional mechanical recycling schemes owing to their multilayer architecture [3, 4]. Worldwide, several tens of thousands of tonnes of obsolete CDs and DVDs are landfilled or incinerated annually without any material recovery, representing both an environmental burden and an underexploited carbon-rich feedstock [5, 6]. Converting waste materials into high-value functional products is a cornerstone strategy of the circular economy [7]. Porous carbons are among the most commercially significant outputs of waste valorization, given their applications in water treatment, gas separation, energy storage, and catalysis [8, 9]. In particular, chemical activation of carbon-rich precursors with alkaline hydroxides is well established as a route to materials with tailored microporosity and surface functionality [10–13]. The mechanism involves dehydration of surface oxygen groups, redox reactions between the carbon matrix and the hydroxide melt, and intercalation of potassium (or other alkali metal) species into the graphene layers, followed by their

release during washing—a process that expands the incipient pore system [14–16]. Among alkaline activating agents, KOH has been most widely studied and is recognized for producing highly microporous structures [14–16]. By contrast, LiOH and $Ba(OH)_2$ interact differently with the carbon precursor owing to differences in ionic radius, hydration enthalpy, and melting point, which alter the balance between etching, intercalation, and surface oxidation. Comparative studies on waste-derived precursors activated with these three hydroxides are rare [17, 18], and no systematic investigation has been reported for polycarbonate-based optical media. This gap is particularly relevant because CDs and DVDs differ fundamentally from lignocellulosic precursors: they exhibit a dense and highly uniform polymeric matrix, a distinct decomposition pathway, and limited inherent porosity, all of which are expected to influence both activation mechanisms and the resulting pore architecture.

This work reports the synthesis and comprehensive characterization of activated carbons derived from recycled CDs and DVDs using KOH, LiOH, and $Ba(OH)_2$. The materials are characterized by N_2 and CO_2 adsorption, Raman spectroscopy, FTIR, Boehm titration, point of zero charge, thermogravimetric analysis, and X-ray diffraction. Their adsorption performance toward BTX vapors (benzene, toluene, and xylene) is evaluated in a fixed-bed system, and breakthrough data are interpreted using established dynamic models. The objective is to identify the key parameters governing the transformation of polycarbonate waste into functional porous carbons and to establish a structure–property framework for their rational design.

2. Materials and Methods

2.1 Raw material and pre-treatment

Discarded CDs and DVDs were collected from university and household sources as representative polycarbonate-based electronic waste. The materials were mechanically fragmented and sieved to obtain particles with an average size of approximately 4 mm. Inorganic contaminants and surface impurities were removed by treatment with a 10 wt% HCl solution under ultrasonic agitation, followed by thorough rinsing with deionised water to neutral pH and subsequent drying at 80 °C.

2.2 Carbonisation process

Carbonisation was performed in a tubular furnace under a nitrogen atmosphere to prevent oxidation. The precursor was heated at 5 °C min^{-1} to 500 °C and held at that temperature for 1 h. This step promoted thermal decomposition of the polycarbonate matrix and formation of a carbon-rich char suitable for subsequent chemical activation.

2.3 Chemical activation

The carbonized material was chemically activated with aqueous solutions of KOH, LiOH, and $Ba(OH)_2$ at a 4:1 mass ratio of activating agent to char [19, 20]. The impregnated mixtures were heated to 700 °C for 1 h under a continuous nitrogen flow. After activation, the samples were repeatedly washed with deionized water until neutral pH and then dried at 80 °C. The resulting carbons are referred to as AC-KOH, AC-Ba, and AC-Li throughout the text.

2.4 Characterisation techniques

Textural properties were determined from nitrogen adsorption–desorption isotherms at 77 K and carbon dioxide adsorption isotherms at 273 K, measured on an automated volumetric analyzer [21]. BET surface areas, total pore volumes, and micropore volumes were calculated using established protocols [11, 12]. Pore size distributions were obtained by applying density functional theory (DFT) to the N_2 adsorption branch [13, 14]. Structural order was assessed by Raman spectroscopy (532 nm excitation). Surface functional groups were identified by FTIR spectroscopy and quantified by Boehm titration with $NaHCO_3$, Na_2CO_3, NaOH, and HCl solutions [19, 20]. The point of zero charge (pH_{pzc}) was determined by the pH-drift method [21]. Thermal stability was evaluated by thermogravimetric analysis (TGA) under nitrogen from 25 to 900 °C at 10 °C min^{-1}.

2.5 Kinetic analysis of BTX vapor adsorption

BTX vapor adsorption kinetics were evaluated in a continuous fixed-bed system under controlled gas-phase conditions. A defined mass of activated carbon was packed into a quartz column and pre-treated under inert gas to remove moisture. A BTX-containing feed stream at constant concentration was introduced at fixed temperature and volumetric flow rate. Outlet concentration was monitored continuously and adsorption performance was represented as breakthrough curves (C/C_0 vs. time). Breakthrough time, saturation time, and mass-transfer zone length were determined from these profiles. The dynamic behaviour was analysed using the Thomas [22], Yoon–Nelson [23], and Bohart–Adams [24] equations. In particular, the Thomas model was applied as:

$$\ln\left(\frac{C_0}{C}-1\right)=\frac{k^{th}q_0m}{Q}-k_{\mathrm{Th}}C_0t$$

where k^{Th} is the Thomas rate constant, q_0 is the maximum adsorption capacity, m is the mass of adsorbent, Q is the volumetric flow rate, C_0 is the inlet concentration, and t is time. A linear driving force (LDF) approximation was additionally used to estimate apparent mass-transfer coefficients and compare effective diffusion rates among the samples.

2.6 Adsorption capacity, separation performance, and modelling

Adsorption capacity (q, mg g^{-1}) was determined from the inlet–outlet mass balance:

$$q\ =\frac{(C_{in}-C_{out})\cdot F\cdot t}{m}$$

where C^{In} and C_o^{Ut} are inlet and outlet concentrations (mg L^{-1}), F is the volumetric flow rate (L min^{-1}), t is the adsorption time (min), and m is the adsorbent mass (g). Kinetic data were fitted to pseudo-first-order (PFO) [25], pseudo-second-order (PSO) [26], Elovich [27], and intraparticle diffusion [28] models. Equilibrium data were described by Langmuir [29] and Freundlich [30] isotherms. Thermodynamic parameters ($\Delta G°$, $\Delta H°$, $\Delta S°$) were estimated from temperature-dependent adsorption data using the Van't Hoff approach [31].

3. Results and Discussion

3.1 Textural characterisation and pore structure: N_2 and CO_2 adsorption

The textural properties of the three activated carbons are summarized in Table 1. The N_2 adsorption–desorption isotherms (Fig. 1a) and the CO_2 adsorption isotherms at 273 K (Fig. 1b) are presented together to provide a complete picture of the pore landscape, because CO_2 at 273 K accesses ultramicropores that remain kinetically inaccessible to N_2 at 77 K [11, 12].

All three isotherms exhibit Type I behavior according to the IUPAC classification [21], with steep uptake at very low relative pressures, indicative of a predominantly microporous structure. The rapid plateau confirms that pore filling occurs almost exclusively within a confined microporous network, with negligible mesopore contribution. AC-KOH shows the highest adsorption capacity across the entire pressure range, consistent with its superior BET surface area (≈ 500 $m^2\ g^{-1}$) and total pore volume (≈ 0.25 $cm^3\ g^{-1}$). AC-Ba and AC-Li show progressively lower uptakes, reflecting the reduced effectiveness of $Ba(OH)_2$ and LiOH as pore-developing agents in this polycarbonate precursor.

Table 1. Textural properties of activated carbons derived from CD/DVD waste as a function of the activating agent.

Activating agent	BET surface area ($m^2\ g^{-1}$)	Total pore volume ($cm^3\ g^{-1}$)	Micropore volume from CO_2 ($cm^3\ g^{-1}$)	Mean pore width (nm)
KOH	500	0.251	0.084	0.38
$Ba(OH)_2$	226	0.093	0.081	0.37
LiOH	157	0.079	0.062	0.37

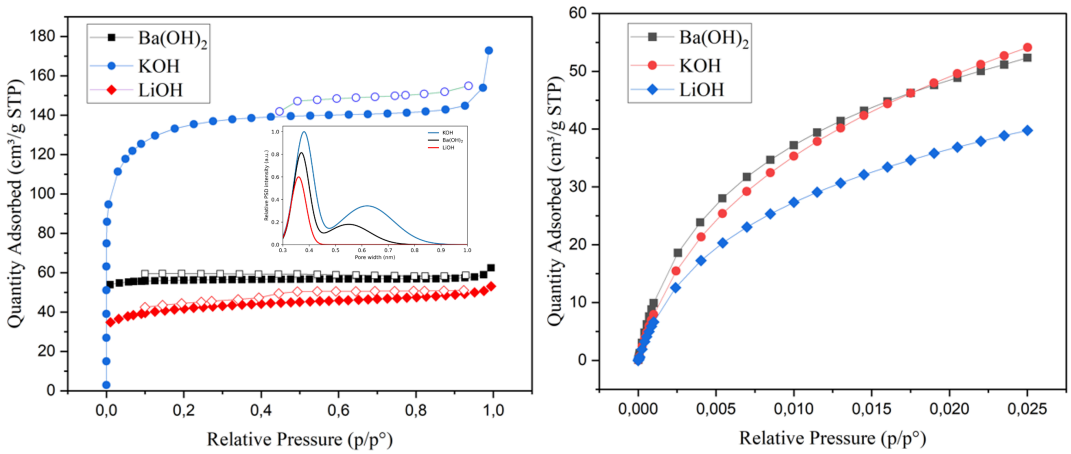

Fig. 1. Adsorption isotherms of activated carbons prepared with different hydroxide activating agents. (a) N_2 adsorption–desorption isotherms at 77 K; the inset shows the pore size distribution (PSD) confirming predominance of ultramicropores centred at 0.35–0.40 nm. (b) CO_2 adsorption isotherms at 273 K, emphasising the ultramicropore contribution inaccessible to N_2 at 77 K.

The CO_2 uptake data confirm the dominant role of ultramicroporosity across all three carbons [29–31]. Mean pore widths of 0.37–0.38 nm (Table 1) fall within the range where overlapping solid–fluid interactions create enhanced adsorption potentials, explaining the steep uptake at very low pressures. The pore size distribution (Fig. 1a, inset) shows a main population centered at 0.35–0.40 nm for all samples, with AC-KOH additionally exhibiting a shoulder extending into the supermicropore range (≈ 0.7–1.0 nm). This broader connectivity is of practical significance because it enables molecular diffusion into the ultramicroporous regions while maintaining strong confinement; it is absent in AC-Ba and AC-Li, which show narrower, more constrained distributions [32–34].

The consistency across N_2 isotherms, CO_2 uptake, pore-size distributions, and the parameters in Table 1 underscores the dominant role of the activating agent in shaping pore architecture. KOH promotes efficient chemical activation, in which potassium intercalation and gasification generate a hierarchical microporous network that combines energetically favorable ultramicropores with accessible transport micropores—a combination that proves particularly advantageous for the adsorption of small aromatic molecules, as discussed in Section 3.4.

3.2 Surface chemistry and functional group distribution

Boehm titration results are summarized in Table 2. Carbon derived from $Ba(OH)_2$ exhibits the highest concentration of basic surface groups (≈ 0.41 mmol g^{-1}), reflecting the strongly basic character of the activating medium and the partial retention of electron-donating functionalities after washing. AC-KOH has lower overall basicity but a more balanced distribution of acidic and basic groups, suggesting a more thorough transformation of the carbon matrix during the high-temperature activation step. AC-Li shows the lowest functional group density, consistent with its underdeveloped textural properties.

Table 2. Surface chemical properties of activated carbons determined by Boehm titration.

Activating agent	Carboxylic groups (mmol g^{-1})	Lactonic groups (mmol g^{-1})	Phenolic groups (mmol g^{-1})	Total acidic groups (mmol g^{-1})	Basic groups (mmol g^{-1})
KOH	0.12	0.09	0.16	0.37	0.32
$Ba(OH)_2$	0.08	0.06	0.11	0.25	0.41
LiOH	0.07	0.05	0.09	0.21	0.24

These differences in surface chemistry are particularly relevant when considered alongside the textural data. The higher basicity of AC-Ba may enhance specific acid–base interactions with acidic adsorbates, and the higher pH_{pzc} values of this carbon (Section 3.3) confirm a positively charged surface over a broader pH range. By contrast, the more balanced surface chemistry of AC-KOH, together with its larger accessible surface area, favors non-specific dispersion forces and π–π interactions [35,36], which are the dominant mechanisms for BTX adsorption on aromatic carbon surfaces.

3.3 Surface chemistry, charge properties, and structural order

FTIR spectra of the three carbons are shown in Fig. 2. A broad absorption band centered at 3200–3600 cm^{-1}, attributable to O–H stretching in hydroxyl groups and adsorbed water, is present in all samples. Bands at 1600–1700 cm^{-1} correspond to C=O stretching in carbonyl and carboxylic species, while signals at 1000–1300 cm^{-1} reflect C–O stretching in phenolic and ether groups. The relative intensity of oxygenated bands decreases in the order AC-Ba > AC-Li > AC-KOH, indicating that the $Ba(OH)_2$-derived carbon retains the most surface oxygen, whereas KOH treatment at 700 °C produces a more extensively reduced carbon matrix. These observations are fully consistent with the Boehm titration data in Table 2.

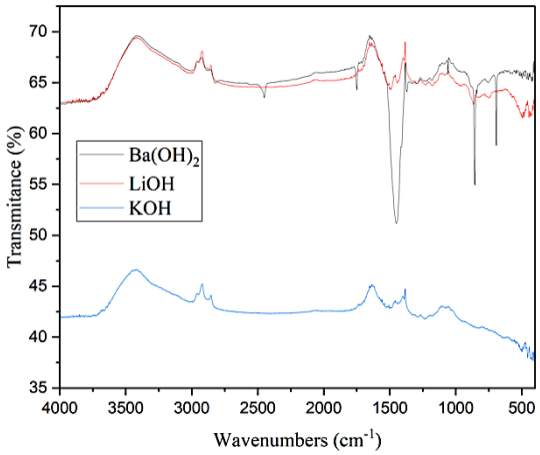

Fig. 2. FTIR spectra of activated carbons prepared with different hydroxide activating agents. Spectra are offset for clarity.

The point of zero charge (pH_{pzc}) profiles are shown in Fig. 3. AC-Ba exhibits the highest pHpzc values across the studied mass range, confirming its predominantly basic surface character. AC-KOH shows intermediate pH_{pzc}, and AC-Li displays values comparable to those of AC-KOH despite having fewer functional groups overall—a result that likely reflects the specific balance between acidic and basic sites rather than their absolute concentration. These surface charge differences have direct implications for adsorption in aqueous or humid environments, where electrostatic interactions modulate adsorbate uptake as a function of solution pH.

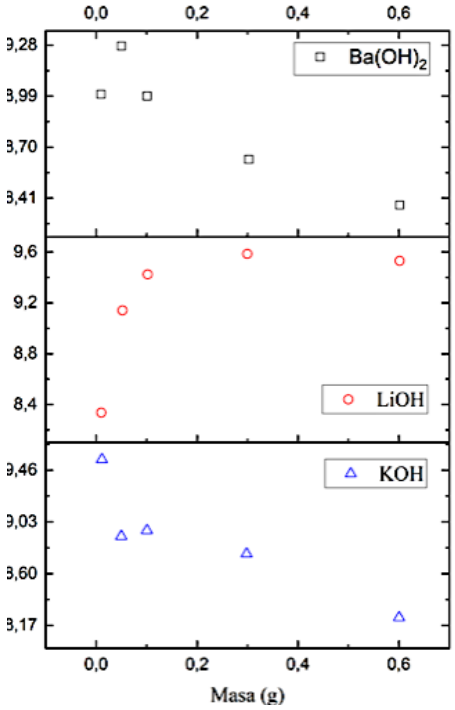

Fig. 3. Point of zero charge (pH_{pzc}) as a function of sample mass for the three activated carbons.

Raman spectra (Fig. 4) show the characteristic D band (~1350 cm^{-1}) and G band (~1580 cm^{-1}) across all materials. The calculated I_D/I_G ratios are essentially identical (~0.84), indicating that the degree of structural disorder is governed by the carbonization step rather than by the chemical activation agent. This finding is important because it demonstrates that the pronounced differences in textural and chemical properties among the three carbons arise from pore-development and surface-modification mechanisms, not from changes in the intrinsic graphitic ordering of the carbon framework.

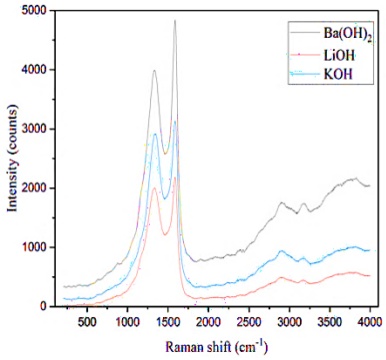

Fig. 4. Raman spectra of the three activated carbons showing D (~1350 cm^{-1}) and G (~1580 cm^{-1}) bands.

TGA curves (Fig. 5) show an initial mass loss below 200 °C, attributed to desorption of physisorbed water, followed by losses between 200 and 600 °C linked to decomposition of surface oxygen groups (consistent with FTIR and Boehm results), and a final stage above 600 °C, where the bulk carbon matrix degrades. AC-KOH retains the highest residual mass at 900 °C, confirming a more condensed and thermally stable carbon structure after intense KOH activation. AC-Ba and AC-Li show progressively greater mass losses, consistent with less extensive graphitization and higher concentrations of surface oxygenates.

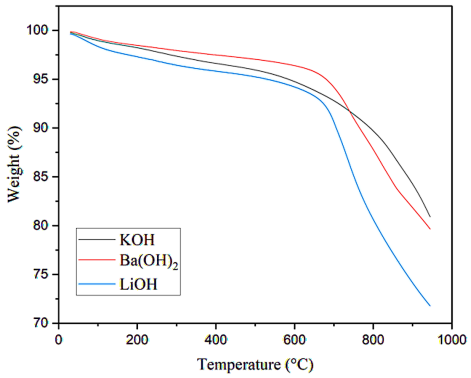

Fig. 5. TGA curves of the three activated carbons under N_2 from 25 to 900 °C.

3.4 Adsorption performance and kinetic analysis toward BTX vapors

BTX adsorption on aromatic carbons involves two principal contributions: confinement within micropores, where overlapping solid–fluid potentials enhance adsorption energy; and π–π interactions between the delocalized electron systems of the aromatic adsorbates and the sp^2 carbon domains of the adsorbent surface [32–34]. Given that all three carbons present comparable I_D/I_J ratios (Section 3.3), differences in BTX uptake should arise primarily from differences in pore accessibility and surface area rather than from variations in graphitic domain quality.

Breakthrough curves for benzene, toluene, and xylene on the three carbons are shown in Fig. 6. AC-KOH displays the longest breakthrough times and the highest adsorption capacities for all three adsorbates, reflecting the favourable combination of high surface area and accessible micropore network identified in Section 3.1. The sharp breakthrough front observed for AC-KOH indicates efficient adsorption dynamics and good coupling between transport and adsorption processes. AC-Li shows markedly earlier breakthrough and lower saturation capacity; AC-Ba occupies an intermediate position, with its higher surface basicity partially compensating for a less developed pore structure.

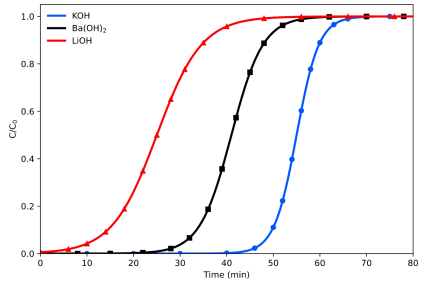

Fig. 6. Breakthrough curves for BTX vapor adsorption on AC-KOH, AC-Ba, and AC-Li. The steeper slope of the AC-KOH curves is indicative of more efficient adsorption dynamics and a shorter mass-transfer zone.

Table 3. Adsorption capacities and breakthrough parameters for BTX compounds on the three activated carbons.

Sample	Benzene capacity (mg g^{-1})	Toluene capacity (mg g^{-1})	Xylene capacity (mg g^{-1})	Breakthrough time (min)	Mass transfer zone (cm)
KOH	185	210	235	48	1.8
$Ba(OH)_2$	120	145	165	32	2.6
LiOH	75	92	110	18	3.8

The adsorption capacities listed in Table 3 confirm the trend observed in the breakthrough curves. Within each carbon, capacities increase in the order benzene < toluene < xylene, consistent with the higher molecular polarisability and boiling point of the heavier BTX components, which strengthen dispersion interactions with the micropore walls [15, 32]. The substantially longer mass-transfer zones of AC-Ba and AC-Li (Table 3) reflect the increasing role of intraparticle diffusion resistance as pore accessibility decreases.

Thomas model fitting (Table 4) corroborates these observations: both the maximum adsorption capacity (q_0) and the Thomas rate constant (k^{Th}) follow the order AC-KOH > AC-Ba > AC-Li. The higher k^{Th} of AC-KOH indicates faster adsorption dynamics, linked to improved micropore connectivity and reduced diffusion resistance in the broader pore network of this carbon.

Table 4. Thomas model parameters for BTX vapor adsorption on the three activated carbons.

Sample	q_o(mg g^{-1})	k_{Th}(min^{-1})
KOH	200	0.050
$Ba(OH)_2$	140	0.035
LiOH	90	0.020

Kinetic fitting results are summarised in Table 5. The PSO model provides the best fit for all three carbons (R^2 > 0.99), suggesting that the rate-controlling step involves surface interactions and chemisorption-like processes at energetically heterogeneous sites [22]. The Elovich model yields good fits as well (Table 5), supporting the presence of a distribution of adsorption energies—particularly broad in AC-KOH, where the diverse pore size distribution provides a range of confinement environments [24].

Table 5. Kinetic parameters for BTX adsorption on the three activated carbons.

Sample	Model	k_1 (min^{-1})	k_2 (g mg^{-1} min^{-1})	$q_{e,exp}$ (mg g^{-1})	$q_{e,calc}$ (mg g^{-1})	R^2
KOH	PFO	0.045	–	210	185	0.945
	PSO	–	2.8×10^{-3}	210	205	0.996
	Elovich	α = 35 mg g^{-1} min^{-1}	β = 0.045 g mg^{-1}	–	–	0.982
$Ba(OH)_2$	PFO	0.031	–	145	125	0.932
	PSO	–	1.9×10^{-3}	145	140	0.993
	Elovich	α = 22	β = 0.052	–	–	0.975
LiOH	PFO	0.018	–	95	80	0.918
	PSO	–	1.1×10^{-3}	95	92	0.991
	Elovich	α = 15	β = 0.061	–	–	0.968

Intraparticle diffusion analysis (Table 6) indicates a multi-stage adsorption process: the plots of q^t vs. $t^{1/2}$ show two linear segments that do not pass through the origin, confirming that intraparticle diffusion is not the sole rate-limiting step [25]. The intercept C (Table 6) represents the contribution of the boundary-layer resistance to the overall adsorption rate; its decrease from AC-KOH to AC-Li reflects the progressively slower external mass transfer in carbons with smaller and less interconnected pore networks.

Table 6. Intraparticle diffusion parameters for BTX adsorption**.**

Sample	k_{id} (mg g^{-1} min$^{-1/2}$)	C (mg g^{-1})	R^2
KOH	22.5	85	0.971

Sample	k_{id} (mg g^{-1} $min^{-1/2}$)	C (mg g^{-1})	R^2
$Ba(OH)_2$	15.8	60	0.965
LiOH	10.2	42	0.958

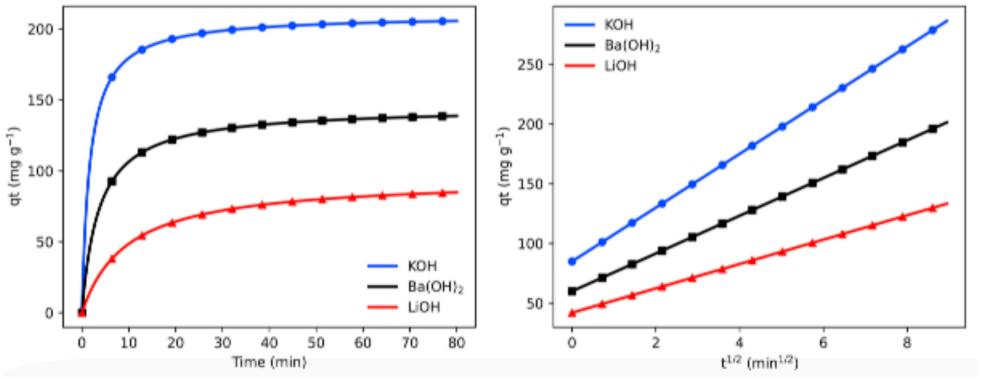

Fig. 7. Kinetic modelling of BTX adsorption. (a) PSO kinetic fit (q^t vs. t); (b) intraparticle diffusion plots (q^t vs. $t^{1/2}$). The non-zero intercepts of the diffusion plots confirm that external mass transfer and surface adsorption both contribute to the overall rate.

Thermodynamic parameters derived from temperature-dependent adsorption data are listed in Table 7. The negative ΔG° values confirm spontaneous adsorption under all conditions studied; the negative ΔH° values (−21 to −32 kJ mol^{-1}) are within the range characteristic of physisorption, consistent with π–π interactions and van der Waals forces as dominant mechanisms. The negative ΔS° values reflect the expected decrease in molecular randomness when BTX molecules are confined within the microporous network.

Table 7. Thermodynamic parameters for BTX adsorption on the three activated carbons.

Sample	ΔG° (kJ mol^{-1})	ΔH° (kJ mol^{-1})	ΔS° (J mol^{-1} K^{-1})
KOH	-18.5	-32.0	-45
$Ba(OH)_2$	-14.2	-27.5	-38
LiOH	-10.8	-21.3	-32

3.5 Mechanistic interpretation and structure–property relationship

Taken together, the adsorption, kinetic, and thermodynamic data provide a coherent mechanistic picture. Adsorption of BTX on the CD/DVD-derived carbons is primarily physisorption, driven by micropore filling and π–π interactions between the aromatic adsorbates and the sp^2 carbon domains of the adsorbent. The superior performance of AC-KOH stems from its well-developed ultramicroporous network, which provides both a high density of energetically favorable adsorption sites and transport pathways to those sites through slightly broader micropores. The broader breakthrough profiles and longer mass-transfer zones of AC-Ba and AC-Li reflect the increasing role of pore-constriction-induced diffusion resistance as micropore connectivity decreases.

Surface chemistry plays a secondary but non-negligible role. The higher basicity of AC-Ba enhances π–π donor–acceptor interactions with the electron-rich aromatic rings of BTX molecules [35, 36], partially offsetting its reduced pore volume. The thermodynamic data are consistent with this picture: the slightly more exothermic adsorption on AC-KOH reflects stronger confinement in narrower ultramicropores rather than stronger chemical bonding.

From a valorization perspective, converting polycarbonate optical media into AC-KOH—a material with a BET surface area of 500 m^2 g^{-1} and BTX capacities exceeding 200 mg g^{-1}—represents a

technically meaningful route to transforming a problematic e-waste fraction into a competitive adsorbent. These performance values compare favorably with activated carbons derived from other plastic wastes reported in the literature [5, 17, 18, 32], reinforcing the viability of the proposed valorization approach.

4. Conclusions

This work demonstrates that polycarbonate-based optical waste, such as discarded CDs and DVDs, can be converted into functional microporous carbons via alkaline chemical activation. The results clearly show that the activating agent governs both pore development and surface chemistry, ultimately determining adsorption performance for BTX vapors. KOH activation produced the most developed porous structure, as reflected by the highest BET surface area (≈ 500 $m^2 g^{-1}$) and a well-connected micropore network. This structural advantage translated directly into superior adsorption behavior, with xylene uptake reaching approximately 235 mg g^{-1}, along with longer breakthrough times and faster adsorption kinetics. Such performance can be rationalized by the well-established KOH activation pathway, which promotes simultaneous carbon gasification and alkali intercalation, leading to efficient pore generation.

In contrast, $Ba(OH)_2$ produced a carbon with a less developed pore system but a more basic surface, as evidenced by Boehm titration and pH_pzc measurements. Although its adsorption capacity was lower, the increased basicity appears to enhance specific interactions with aromatic molecules, partially compensating for the reduced surface area. The material obtained with LiOH showed limited pore formation and, consequently, the lowest adsorption performance across all tested conditions. Raman spectroscopy showed comparable levels of disorder across all samples ($I_D/I_G \approx 0.84$), indicating that the observed differences in adsorption behavior are not linked to changes in graphitic ordering but rather to variations in pore architecture and surface functionality introduced during activation. Kinetic analysis showed that adsorption is best described by the pseudo-second-order model ($R^2 > 0.99$), while intraparticle diffusion plots indicate a multi-step mechanism involving both external mass transfer and diffusion within the pore network. Consistently, fitting breakthrough curves using the Thomas model highlights the critical role of micropore accessibility in controlling dynamic adsorption performance.

From a broader perspective, these results provide a clear structure–property relationship linking activation chemistry, pore development, and adsorption efficiency in carbons derived from polycarbonate waste. In practical terms, KOH activation at 700 °C with a 4:1 reagent-to-carbon ratio emerges as the most effective route for producing high-performance BTX adsorbents. More generally, this study reinforces the potential of electronic polymer waste as a viable precursor for advanced carbon materials within a circular economy framework.

Acknowledgements

The authors acknowledge the framework agreement between Universidad de los Andes and the Universidad Nacional de Colombia (Bogotá Campus). Financial support from the Faculty of Sciences at Universidad de los Andes under project INV-2025-213-3457 is gratefully acknowledged.

References

1. Baldé, C.P., Forti, V., Gray, V., Kuehr, R., Stegmann, P.: *The Global E-Waste Monitor 2020: Quantities, Flows, and the Circular Economy Potential.* United Nations University / United Nations Institute for Training and Research, Bonn/Geneva/Rotterdam (2020). https://doi.org/10.53332/2020-047
2. Forti, V., Baldé, C.P., Kuehr, R., Bel, G.: *The Global E-Waste Monitor 2020.* International Telecommunication Union, Geneva (2020). https://www.itu.int/pub/D-INDC-EEPP-2020

3. Menad, N., Guignot, S., van Houwelingen, J.A.: New characterisation method of electrical and electronic equipment wastes (WEEE). *Waste Manag.* 33, 706–713 (2013). https://doi.org/10.1016/j.wasman.2012.09.023
4. Oguchi, M., Mamoto, S., Sakanakura, H., Kida, A.: A preliminary categorization of end-of-life electrical and electronic equipment as secondary metal resources. *Waste Manag.* 31, 2150–2160 (2011). https://doi.org/10.1016/j.wasman.2011.05.009
5. Matos, I., Fernandes, S., Guerreiro, L., Barata, S., Ramos, A.M., Vital, J., Fonseca, I.M.: The effect of surfactants on the porosity of activated carbons prepared from plastic waste. *Microporous Mesoporous Mater.* 92, 38–46 (2006). https://doi.org/10.1016/j.micromeso.2005.12.009
6. Xiao, R., Chen, Y., Zhang, H.: Pyrolysis of CDs and DVDs and their polycarbonate-rich mixtures: product distributions and characterisation. *J. Anal. Appl. Pyrolysis* 93, 135–140 (2012). https://doi.org/10.1016/j.jaap.2011.10.009
7. Ellen MacArthur Foundation: *Towards the Circular Economy: Economic and Business Rationale for an Accelerated Transition.* Ellen MacArthur Foundation, Isle of Wight (2013). https://www.ellenmacarthurfoundation.org/towards-the-circular-economy
8. Wang, J., Kaskel, S.: KOH activation of carbon-based materials for energy storage. *J. Mater. Chem.* 22, 23710–23725 (2012). https://doi.org/10.1039/C2JM34066F
9. Foo, K.Y., Hameed, B.H.: Preparation and characterisation of activated carbon from biomass and its application in adsorption. *Chem. Eng. J.* 170, 411–421 (2011). https://doi.org/10.1016/j.cej.2011.03.119
10. Ioannidou, O., Zabaniotou, A.: Agricultural residues as precursors for activated carbon production—a review. *Renew. Sustain. Energy Rev.* 11, 1966–2005 (2007). https://doi.org/10.1016/j.rser.2006.03.013
11. Dubinin, M.M.: Fundamentals of the theory of adsorption in micropores of carbon adsorbents. *Carbon* 27, 457–467 (1989). https://doi.org/10.1016/0008-6223(89)90010-8
12. Lastoskie, C., Gubbins, K.E., Quirke, N.: Pore size distribution analysis of microporous carbons: a density functional theory approach. *J. Phys. Chem.* 97, 4786–4796 (1993). https://doi.org/10.1021/j100140a025
13. Jagiello, J., Thommes, M.: Comparison of DFT characterization methods based on N_2, Ar, CO_2, and H_2 adsorption. *Carbon* 42, 1227–1232 (2004). https://doi.org/10.1016/j.carbon.2004.03.022
14. Lillo-Ródenas, M.A., Cazorla-Amorós, D., Linares-Solano, A.: Understanding chemical reactions between carbons and NaOH and KOH. *Carbon* 41, 267–275 (2003). https://doi.org/10.1016/S0008-6223(02)00317-3
15. Moreno-Castilla, C.: Adsorption of organic molecules from aqueous solutions on carbon materials. *Carbon* 42, 83–94 (2004). https://doi.org/10.1016/j.carbon.2003.09.022
16. Bansal, R.C., Goyal, M.: *Activated Carbon Adsorption.* CRC Press, Boca Raton (2005). https://doi.org/10.1201/9781420028812
17. Pelekani, C., Snoeyink, V.L.: Competitive adsorption in natural water: role of activated carbon pore size. *Carbon* 37, 1423–1430 (1999). https://doi.org/10.1016/S0008-6223(99)00038-5
18. Li, W., Zhang, L., Peng, J., Li, N., Zhu, X.: Preparation of high surface area activated carbons from tobacco stems with K_2CO_3 activation using microwave radiation. *Ind. Crops Prod.* 27, 341–347 (2008). https://doi.org/10.1016/j.indcrop.2007.11.016
19. Boehm, H.P.: Some aspects of the surface chemistry of carbon blacks and other carbons. *Carbon* 32, 759–769 (1994). https://doi.org/10.1016/0008-6223(94)90031-0

20. Figueiredo, J.L., Pereira, M.F.R., Freitas, M.M.A., Órfão, J.J.M.: Modification of the surface chemistry of activated carbons. *Carbon* 37, 1379–1389 (1999). https://doi.org/10.1016/S0008-6223(98)00200-9

21. Thommes, M., Kaneko, K., Neimark, A.V., Olivier, J.P., Rodriguez-Reinoso, F., Rouquerol, J., Sing, K.S.W.: Physisorption of gases, with special reference to the evaluation of surface area and pore size distribution (IUPAC Technical Report). *Pure Appl. Chem.* 87, 1051–1069 (2015). https://doi.org/10.1515/pac-2014-1117

22. Thomas, H.C. Heterogeneous ion exchange in a flowing system. *Journal of the American Chemical Society* 66 (1944) 1664–1666. https://doi.org/10.1021/ja01238a017

23. Yoon, Y.H., Nelson, J.H.Application of gas adsorption kinetics I. A theoretical model for respirator cartridge service life. *American Industrial Hygiene Association Journal* 45 (1984) 509–516. https://doi.org/10.1080/15298668491400197

24. Bohart, G.S., Adams, E.Q. Some aspects of the behavior of charcoal with respect to chlorine. *Journal of the American Chemical Society* 42 (1920) 523–544. https://doi.org/10.1021/ja01448a018

25. Lagergren, S.: Zur Theorie der sogenannten Adsorption gelöster Stoffe. *Kungliga Svenska Vetenskapsakad. Handlingar* 24, 1–39 (1898).

26. Ho, Y. S., McKay, G.: Pseudo-second order model for sorption processes. *Process Biochem.* 34, 451–465 (1999). https://doi.org/10.1016/S0032-9592(98)00112-5

27. Elovich, S.Y., Larinov, O.G. Theory of adsorption from solutions of nonelectrolytes on solid adsorbents. *Izvestiya Akademii Nauk SSSR, Otdelenie Khimicheskikh Nauk* (1962) 209–216.

28. Weber, W.J., Morris, J.C.: Kinetics of adsorption on carbon from solution. *J. Sanit. Eng. Div.* 89(2), 31–60 (1963). https://doi.org/10.1061/JSEDAI.0000430

29. Langmuir, I.: The adsorption of gases on plane surfaces of glass, mica, and platinum. *J. Am. Chem. Soc.* 40, 1361–1403 (1918). https://doi.org/10.1021/ja02242a004

30. Freundlich, H.: Über die Adsorption in Lösungen. *Z. Phys. Chem.* 57, 385–470 (1906).

31. Azizian, S.: Kinetic models of sorption: a theoretical analysis. *J. Colloid Interface Sci.* 276, 47–52 (2004). https://doi.org/10.1016/j.jcis.2004.03.048

32. Foo, K.Y., Hameed, B.H.: Insights into the modelling of adsorption isotherm systems. *Chem. Eng. J.* 156, 2–10 (2010). https://doi.org/10.1016/j.cej.2009.12.019

33. Dąbrowski, A.: Adsorption—from theory to practice. *Adv. Colloid Interface Sci.* 93, 135–224 (2001). https://doi.org/10.1016/S0001-8686(00)00082-8

34. Ruthven, D.M.: *Principles of Adsorption and Adsorption Processes.* Wiley, New York (1984).

35. Sevilla, M., Fuertes, A.B.: Sustainable porous carbons with a superior performance for CO_2 capture. *Energy Environ. Sci.* 4, 1765–1771 (2011). https://doi.org/10.1039/C0EE00388K

36. Sahmoune, M.N. Evaluation of thermodynamic parameters for adsorption of heavy metals by green adsorbents. *Environmental Chemistry Letters* 17 (2019) 697–704. https://doi.org/10.1007/s10311-018-00819-z

37. Lua, A.C., Yang, T.: Characteristics of activated carbon prepared from pistachio-nut shell by zinc chloride activation under nitrogen and vacuum conditions. *J. Colloid Interface Sci.* 274, 594–601 (2004). https://doi.org/10.1016/j.jcis.2004.04.015

38. Marsh, H., Rodríguez-Reinoso, F.: *Activated Carbon.* Elsevier, Amsterdam (2006). https://doi.org/10.1016/B978-0-08-044463-5.X5000-9

39. Li, X., Zhang, L., Yang, Z., Wang, P., Yan, Y., Ran, J.: Adsorption materials for volatile organic compounds (VOCs) and the key factors for VOC adsorption: a review. *Sep. Purif. Technol.* 235, 116213 (2020). https://doi.org/10.1016/j.seppur.2019.116213
40. Radovic, L.R., Moreno-Castilla, C., Rivera-Utrilla, J.: Carbon materials as adsorbents in aqueous solutions. In: Radovic, L.R. (ed.) *Chemistry and Physics of Carbon*, vol. 27, pp. 227–405. Marcel Dekker, New York (2000).
41. Patel, H.: Fixed-bed column adsorption study: a comprehensive review. *Appl. Water Sci.* 9, 45 (2019). https://doi.org/10.1007/s13201-019-0927-7
42. Tsai, W.T., Chang, C.Y., Ing, C.H., Chang, C.F. Simplified description of adsorption breakthrough curves of 1,1-dichloro-1-fluoroethane on activated carbon. *Journal of Colloid and Interface Science* 214 (1999) 455–458. https://doi.org/10.1006/jcis.1999.6192
43. Hu, Q., Pang, S., Wang, D., Yang, Y., Liu, H. Deeper insights into the Bohart–Adams model in a fixed-bed column. *Journal of Physical Chemistry B* 125 (2021) 8494–8501. https://doi.org/10.1021/acs.jpcb.1c03378
44. Crank, J.: *The Mathematics of Diffusion,* 2nd edn. Oxford University Press, Oxford (1975).
45. Rouquerol, F., Rouquerol, J., Sing, K.S.W., Llewellyn, P., Maurin, G.: *Adsorption by Powders and Porous Solids: Principles, Methodology and Applications,* 2nd edn. Academic Press, Oxford (2014). https://doi.org/10.1016/C2013-0-15309-6